Adaptive Regulation of Vector-Controlled Induction Motors

Fabrice Jadot, Francois Malrait, Javier Moreno-Valenzuela, and Rodolphe Sepulchre, *Member, IEEE*

***Abstract*—This paper addresses the speed and flux regulation of induction motors under the assumption that the motor parameters are poorly known. An adaptive passivity-based control is proposed that guarantees robust regulation as well as accurate estimation of the electrical parameters that govern the motor performance. This paper provides a local stability analysis of the adaptive scheme, which is illustrated by simulations and supported by a successful experimental validation on an industrial product.**

I. Introduction

MODEL-BASED induction motor control for high-performance drives has motivated an impressive amount of research over the last decades. The development of commercial vector-controlled induction motors has been primarily based on the principle of field orientation which offers an elegant way to decouple the motor torque and flux regulation [1],[2]. Several books illustrate the subsequent theoretical and practical advances of this active research field [3]–[5].

Because induction motors are mass products commercialized in very different sizes and for very different applications, a challenge for the variable-speed-drive industry is to develop performant yet versatile control algorithms. In order to justify the cost of sensors and computer-control technology, the closed-loop performance must outperform the performance of simpler products. At the same time, the controller performance must minimally rely upon the features of a particular product (i.e., the motor electrical and mechanical parameters) because most applications do not justify the cost of precise and on-site commissioning by the drive manufacturer. It is of interest for the research control community to demonstrate that model-based nonlinear control methods developed in the last two decades, e.g., feedback linearization methods [6], [7], Lyapunov-based control [8], [9], and passivity-based methods [10], [11], provide guidelines and tools to reach that objective. The electromechanical model of the induction motor is reliable and of moderate complexity, but it is nonlinear and contains several uncertain parameters. Induction motor control applications pose a number of additional challenges, including the measurement of a restricted number of state variables, amplitude constraints on state and control variables, and the rapid variation of reference signals across a wide range of operating conditions. Particular success has been demonstrated for the passivity-based methods that exploit the physical dissipativity properties of the motor [12]–[14]. These methods provide robust output feedback schemes that closely match the long-established concept of field-oriented control in the industry [15], [16]. They are amenable to Lyapunov analysis, which has been exploited, for instance, in the design of adaptive controllers that compensate for the parametric uncertainty associated with the mechanical load[17].

Model-based control methods for induction motors all require reasonable knowledge about four independent electrical parameters of the motors [two (equivalent) resistances and two (equivalent) inductances]. It is well known that these parameters are poorly known in applications and that resistances undergo drastic thermic variations during normal operation of the motor. The resulting parametric uncertainty not only exposes the robustness of the model-based control schemes but also deteriorates the closed-loop performance of the motor. Accurate estimation of the electrical parameters is, for instance, necessary for load torque estimation and for operation at the desired current, two industrial concerns for high-performance drives. For these reasons, the issue of parametric estimation has been addressed by a number of authors (see, e.g.,[18]–[21] and the references therein). Marino *et al.* have provided a ninth-order estimation scheme that provides online estimation of the stator and rotor resistance [20]. They also proposed an adaptive control scheme that provides an estimation of the rotor resistance and of the load torque [21]. The latter result nevertheless requires the knowledge of the stator resistance and the mechanical inertia, two poorly known parameters in industrial applications.

This paper proposes an adaptive design that guarantees speed and flux robust regulation and, at the same time, accurate estimation of all electrical parameters of interest. The control uses the measurement of the currents and of the mechanical speed. In contrast, no precise knowledge of the electrical and mechanical parameters is required. The controller is shown to achieve local exponential convergence of the unbiased equilibrium under weak persistence of excitation condition. Even when this condition does not hold, the controller achieves in most operating conditions both regulation of the electromechanical variables and accurate estimation of the two most critical electrical parameters (the rotor resistance and an equivalent inductance). The stability analysis is supported by simulation results and by a successful implementation on an industrial product. The theoretical developments of this paper are relatively straight-

Manuscript received July 02, 2008. Manuscript received in final form July 30, 2008. First published April 14, 2009; current version published April 24, 2009. Recommended by Associate Editor S. Peresada.

F. Jadot and F. Malrait are with Schneider Toshiba Inverter Europe (STIE), 27120 Pacy-sur-Eure, France (e-mail: fabrice.jadot@schneider-electric.com; francois.malrait@schneider-electric.com).

J. Moreno-Valenzuela is with the Centro de Investigacin y Desarrollo de Tecnología Digital del Instituto Politécnico Nacional (CITEDI-IPN), 22510 Tijuana, Mexico (e-mail: moreno@citedi.mx).

R. Sepulchre is with the Department of Electrical Engineering and Computer Science, Université de Liège, 4000 Liège Sart Tilman, Belgium (e-mail: r.sepulchre@ulg.ac.be).

Color versions of one or more of the figures in this paper are available online at http://ieeexplore.ieee.org.

Digital Object Identifier 10.1109/TCST.2008.2003434

1063-6536/$25.00 © 2009 IEEE

Authorized licensed use limited to: Rodolphe Sepulchre. Downloaded on May 8, 2009 at 00:30 from IEEE Xplore. Restrictions apply.

TABLE I
PARAMETERS OF THE INDUCTION MOTOR

Parameter	*notation*	*numerical value used in paper*
Rotor inductance	L_r	0.16 mH
Stator inductance	L_s	0.16 mH
Mutual inductance	L_m	0.156 mH
Rotor resistance	R_r	0.9 Ω
Stator resistance	R_s	1.5 Ω
Motor shaft inertia	J	0.045 $kg\,m^2$
Torque load	τ_L	26 $N\,m$
Number of pole pairs	n_p	2

forward. The motor model and its dependence on unknown parameters are recalled in Section II. In the absence of parametric adaptation, the controller design follows in essence the passivity approach developed by Ortega *et al.* [12]–[14], with an extra proportional–integral (PI) control loop for regulation of the currents and of the mechanical speed. These developments are summarized in Section III. The integral variables of the controller provide the basis for two different adaptive schemes proposed in Section IV. The parametric sensitivity of both the adaptation scheme and the static closed-loop performance is studied in Section V, and the discussion is illustrated by simulation results. Section VI presents a simplified adaptation scheme and its experimental validation in an industrial product.

II. MOTOR MODEL AND MODEL PARAMETERIZATION

The induction motor model (following the classical development in [2]) is conveniently written in a frame rotating at speed ω_s (d–q model) as the following fifth-order nonlinear state-space model:

$$\frac{J}{n_p}\frac{\mathrm{d}}{\mathrm{d}t}\omega_r = \frac{3n_p}{2}\frac{L_m}{L_r}\langle i_s, \jmath\psi_r\rangle - \tau_L \tag{1}$$

$$\frac{\mathrm{d}}{\mathrm{d}t}\psi_s = -\jmath\omega_s\psi_s - R_s i_s + u_s \tag{2}$$

$$\frac{\mathrm{d}}{\mathrm{d}t}\psi_r = -\jmath\omega_s\psi_r - R_r i_r + \jmath\omega_r\psi_r \tag{3}$$

with the five state variables ω_r (n_p times the mechanical speed), $\psi_s = \psi_{sd} + \jmath\psi_{sq}$ (stator flux), and $\psi_r = \psi_{rd} + \jmath\psi_{rq}$ (rotor flux). The flux variables are linked to the current variables i_s (stator) and i_r (rotor) by the algebraic relationships

$$\begin{aligned}\psi_s &= L_s i_s + L_m i_r\\ \psi_r &= L_m i_s + L_r i_r.\end{aligned} \tag{4}$$

We use the notation $\langle a, b\rangle = Re\{a\bar{b}\}$ for the standard inner product in $\mathbf{C}$. Disregarding the mechanical equation (1), which will not be used in the control design, the model contains five (electrical) parameters listed in Table I: the resistances R_s (stator) and R_r (rotor) and the inductances L_s (stator), L_r (rotor), and L_m (mutual). Because these parameters are poorly known in most applications, the dependence of the control law in those parameters is critical for the robustness of the design.

As a first observation, we note that the dependence of the design in unknown parameters can be reduced to four independent parameters by rewriting the electrical part of the model (2) in the variables i_s (stator current) and $\varphi_r := L_m/L_r\psi_r$ (equivalent rotor flux). In those variables, (2) is rewritten as

$$\begin{aligned}\frac{\mathrm{d}}{\mathrm{d}t}\varphi_r &= -\left[T_r^{-1} + \jmath[\omega_s - \omega_r]\right]\varphi_r + R_{\mathrm{req}} i_s\\ L_f\frac{\mathrm{d}}{\mathrm{d}t}i_s &= -\left[R_s + R_{\mathrm{req}} + \jmath L_f\omega_s\right] i_s\\ &\quad + \left[T_r^{-1} - \jmath\omega_r\right]\varphi_r + u_s\end{aligned} \tag{5}$$

which only depends on the following four parameters:

$$R_{\mathrm{req}} = R_r\frac{L_m^2}{L_r^2},\quad T_r^{-1} = \frac{R_r}{L_r},\quad R_s,\quad L_f = L_s - \frac{L_m^2}{L_r}. \tag{6}$$

Alternatively, the model can be expressed in the four parameters

$$R_{\mathrm{req}} = R_r\frac{L_m^2}{L_r^2},\quad L = \frac{L_m^2}{L_r},\quad R_s,\quad L_f = L_s - \frac{L_m^2}{L_r} \tag{7}$$

because $T_r^{-1} = R_{\mathrm{req}}/L$. The adaptation scheme proposed in Section IV will be based on the four parameters defined in (7). In the sequel, we use the notation $\omega_g = \omega_s - \omega_r$ for the slip velocity.

III. CONTROL DESIGN WITH PERFECT KNOWLEDGE OF THE PARAMETERS

In this section, we assume that the four electrical parameters defined in (7) are perfectly known. The control objective is to regulate the speed ω_r to a desired value ω_r^{cons} and the flux norm $|\varphi_r|$ to a desired value φ^{cons} in spite of the unknown load torque τ_L. For the theoretical developments, the set points ω_r^{cons} and φ^{cons} and the load torque are assumed piecewise constant. The physical input variables are the stator voltages $u_s = u_{sd} + \jmath u_{sq}$. The pulsation ω_s of the rotating frame is an extra design parameter.

The proposed design is decomposed into the following three steps. First, the current set point is selected according to the classical field-oriented control paradigm (Section III-A). Then, it is shown that this set-point current achieves global regulation of the flux and speed in a current-fed machine (Section III-B). Finally, a voltage-tracking controller is proposed to achieve regulation of the current variables to the desired set point, leading to a complete control scheme that achieves the regulation objective in an arbitrarily large compact set of initial conditions (Section III-C).

A. Field-Oriented Control

Field-oriented control aims at aligning the flux φ_r to the d-axis of the rotating frame, i.e., regulating φ_{rq} to $\varphi_{rq}^{\mathrm{cons}} = 0$. Under the assumption of field orientation ($\varphi_{rq} = 0$), the flux dynamics reduce to the scalar equation

$$\dot{\varphi}_{rd} = -T_r^{-1}\varphi_{rd} + R_{\mathrm{req}} i_{sd} \tag{8}$$

while the mechanical equation becomes

$$\frac{\mathrm{d}}{\mathrm{d}t}\omega_r = \frac{3n_p^2}{2J}\varphi_{rd} i_{sq} - \frac{n_p\tau_L}{J}. \tag{9}$$

Authorized licensed use limited to: Rodolphe Sepulchre. Downloaded on May 8, 2009 at 00:30 from IEEE Xplore. Restrictions apply.

Flux regulation is then achieved by regulating the current i_{sd} to

$$i_{sd}^{\text{cons}} = \frac{T_r^{-1}}{R_{\text{req}}}\varphi^{\text{cons}} \tag{10}$$

while speed regulation is achieved by regulation of the current i_{sq} to

$$i_{sq}^{\text{cons}} = \frac{\hat{\tau}_L}{\frac{3n_p}{2}\varphi^{\text{cons}}}. \tag{11}$$

Because the load torque is unknown, the estimate $\hat{\tau}_L$ is typically provided by PI control of the velocity error $\Delta\omega_r = \omega_r - \omega_r^{\text{cons}}$, i.e.,

$$\begin{cases} R_{\text{req}} i_{sq}^{\text{cons}} = R_{\text{req}} \frac{\hat{\tau}_L}{\frac{3n_p}{2}\varphi^{\text{cons}}} = -k_p[\Delta\omega + \xi]\varphi^{\text{cons}} \\ \dot{\xi} = k_i \Delta\omega. \end{cases} \tag{12}$$

Exact field orientation thus provides a convenient way to decouple the flux regulation from the speed regulation. With full state feedback, field orientation is achieved by choosing the frame velocity ω_s as

$$\omega_s = \omega_r + R_{\text{req}} \frac{i_{sq}}{\varphi_{rd}} \tag{13}$$

which results in the stable decoupled dynamics $\dot{\varphi}_{rq} = -T_r^{-1}\varphi_{rq}$. Because the flux is not measured, we instead select

$$\omega_s = \omega_r + R_{\text{req}} \frac{i_{sq}^{\text{cons}}}{\varphi^{\text{cons}}} \left(= \omega_r + R_{\text{req}} \frac{\hat{\tau}_L}{\frac{3n_p}{2}(\varphi^{\text{cons}})^2} \right). \tag{14}$$

As a consequence of (14) and (10), the following relationship holds between the current set point i_s^{cons} and the flux set point φ_r^{cons}:

$$R_{\text{req}} i_s^{\text{cons}} = \left[T_r^{-1} + \jmath\omega_g\right] \varphi_r^{\text{cons}}. \tag{15}$$

B. Convergence Analysis for Current-Fed Machines

In a current-fed machine, the current i_s can be directly controlled to (10) and (11). The resulting closed-loop dynamics are given by

$$\begin{aligned} \frac{\mathrm{d}}{\mathrm{d}t}\xi &= k_i \Delta\omega \\ \frac{\mathrm{d}}{\mathrm{d}t}\Delta\omega &= \kappa \langle R_{\text{req}} i_s, \jmath\varphi_r \rangle - \frac{n_p \tau_L}{J} \\ \frac{\mathrm{d}}{\mathrm{d}t}\varphi_r &= -\left[T_r^{-1} + \jmath[k_p[\Delta\omega + \xi]]\right]\varphi_r + R_{\text{req}} i_s \end{aligned} \tag{16}$$

with $\kappa := 3n_p^2/2JR_{\text{req}}$ and $i_s := i_s^{\text{cons}}$ given by (15). The dynamics (16) correspond to the closed-loop system obtained with the passivity-based control introduced in [22] for current-fed machines. The desired equilibrium is globally asymptotically stable. See [15] for experimental validation and its relationship to the standard (indirect) field-oriented controller.

C. Current Regulation in Voltage-Controlled Machines

In a voltage-controlled machine, regulation of the current to the set point (15) is achieved through a reference generator for the fluxes and currents

$$\frac{\mathrm{d}}{\mathrm{d}t}\varphi_r^{\text{ref}} = -\left[T_r^{-1} + \jmath\omega_g\right]\varphi_r^{\text{ref}} + R_{\text{req}} i_s^{\text{ref}} - v_r \tag{17}$$

$$\begin{aligned} L_f \frac{\mathrm{d}}{\mathrm{d}t} i_s^{\text{ref}} = &-[R_s + R_{\text{req}} + \jmath L_f \omega_s] i_s^{\text{ref}} \\ &+ \left[T_r^{-1} - \jmath\omega_r\right]\varphi_r^{\text{ref}} + u_s - v_s. \end{aligned} \tag{18}$$

The auxiliary inputs v_r and v_s are to be designed later. The stator voltage u_s is thus selected as

$$\begin{aligned} u_s = &[R_s + R_{\text{req}} + \jmath L_f \omega_s] i_s^{\text{ref}} \\ &- \left[T_r^{-1} - \jmath\omega_r\right]\varphi_r^{\text{ref}} + v_s + \frac{\mathrm{d}}{\mathrm{d}t} L_f i_s^{\text{ref}}. \end{aligned} \tag{19}$$

The first-order reference dynamics

$$L_f \frac{\mathrm{d}i_s^{\text{ref}}}{\mathrm{d}t} = [R_s + R_{\text{req}}]\left(i_s^{\text{cons}} - i_s^{\text{ref}}\right) \tag{20}$$

is selected for the current variables. The control law (19), (17), (20) is a dynamic output-feedback control that generates the following dynamics for the error variables $\Delta i_s = i_s - i_s^{\text{ref}}$ and $\Delta\varphi_r = \varphi_r - \varphi_r^{\text{ref}}$:

$$\begin{aligned} \frac{\mathrm{d}}{\mathrm{d}t}\Delta\varphi_r &= -\left[T_r^{-1} + \jmath\omega_g\right]\Delta\varphi_r + R_{req}\Delta i_s + v_r \\ L_f \frac{\mathrm{d}}{\mathrm{d}t}\Delta i_s &= -[R_s + R_{\text{req}} + \jmath L_f \omega_s]\Delta i_s \\ &\quad + \left[T_r^{-1} - \jmath\omega_r\right]\Delta\varphi_r + v_s. \end{aligned} \tag{21}$$

The auxiliary controls v_r and v_s are now designed so as to achieve robust regulation of the error dynamics. The control law

$$v_r = \left[-R_{\text{req}} - \lambda[T_r^{-1} + \jmath\omega_r]\right]\Delta i_s, \qquad \lambda > 0 \tag{22}$$

achieves strict passivity from v_s to Δi_s, as shown by the storage function

$$V = \frac{1}{2}|\Delta\varphi_r|^2 + \frac{\lambda}{2} L_f |\Delta i_s|^2 \tag{23}$$

which satisfies

$$\dot{V} = -T_r^{-1}|\Delta\varphi_r|^2 - \lambda[R_s + R_{\text{req}}]|\Delta i_s|^2 + \lambda\langle \Delta i_s, v_s \rangle. \tag{24}$$

Strict passivity from v_s to Δi_s implies robust stabilizability by output feedback (see, for instance, [9, Sec. 3.3]). In particular, a PI control

$$\begin{cases} v_s = -K_P[\Delta i_s + \eta] \\ \dot{\eta} = K_I \Delta i_s \end{cases} \tag{25}$$

achieves global convergence of the error system to zero for any K_P,$K_I > 0$. As a consequence, one obtains the following result.

Proposition 1: Assume a time-scale separation between the current dynamics (20) and the current-fed dynamics (16). Then, the controller determined by the stator voltage (19), the reference trajectories (17) and (18), and the output feedback (22),

Authorized licensed use limited to: Rodolphe Sepulchre. Downloaded on May 8, 2009 at 00:30 from IEEE Xplore. Restrictions apply.

(25), and (12) achieves exponential regulation of the flux and of the mechanical speed for any constant reference $(\varphi^{cons}, \omega_r^{\rm cons})$ and any constant load torque τ_L.

Proof: The closed-loop dynamics are the cascade of the error dynamics (21) with output Δi_s and the system

$$\begin{aligned}
\dot{\xi} &= k_i \Delta\omega \\
\dot{\Delta\omega} &= \kappa \left\langle R_{\rm req}\left(i_s^{\rm ref} + \Delta i_s\right), \jmath\varphi_r \right\rangle - \frac{n_p \tau_L}{J} \\
\dot{\varphi}_r &= -\left[T_r^{-1} + \jmath k_p[\Delta\omega + \xi]\right]\varphi_r + R_{\rm req}(i_s^{\rm ref} + \Delta i_s) \\
L_f \frac{{\rm d}i_s^{\rm ref}}{{\rm d}t} &= [R_s + R_{\rm req}]\left(i_s^{\rm cons} - i_s^{\rm ref}\right)
\end{aligned} \tag{26}$$

with input Δi_s. From the Lyapunov analysis (23), (24), Δi_s is a bounded signal that is exponentially decaying to zero for any initial condition. The only equilibrium of the closed-loop dynamics therefore satisfies $i_s = i_s^{\rm ref} = i_s^{\rm cons}$, $\varphi_r = \varphi_r^{\rm cons}$, $\omega_r = \omega_r^{\rm cons}$, and it is exponentially stable if the equilibrium of (26) is exponentially stable for $\Delta i_s = 0$. This last property is a direct consequence of the time-scale separation between the current dynamics (20) and the current-fed dynamics (16). For every constant value $i_s^{\rm cons}$, the equilibrium $i_s^{\rm ref} = i_s^{\rm cons}$ of the *fast* subsystem (20) is globally exponentially stable, while for $i_s = i_s^{\rm ref} = i_s^{\rm cons}$, the equilibrium of the *slow* subsystem (16) is globally asymptotically stable and locally exponentially stable. The semiglobal result for the complete system consisting of a globally exponentially stable fast subsystem and a globally asymptotically stable slow subsystem follows from singular perturbation theory (see for instance, [9, Theorem 3.5]).

The controller structure, shown in the block diagram of Fig. 1, leaves considerable flexibility for the design of the gains, which is to be optimized for the dynamic performance. The exponential convergence of the electrical variables to the references $(\varphi_r^{\rm ref}, i_s^{\rm ref})$, regardless of the mechanical variables, is a crucial property of the design. The controller structure closely matches the design proposed in [13], with additional flexibility in the choice of several gains. This flexibility turned to be quite important in our experimental validation of the controller.

IV. Regulation in the Presence of Parametric Uncertainty

The controller proposed in Section III depends on the four electrical parameters (6). In industrial applications, these parameters are poorly known. In addition, the resistances R_s and $R_{\rm req}$ undergo drastic variations in the (slow) thermal time scale. Substituting the parametric estimates $\hat{R}_{\rm eq}$, $\hat{R}_s$, $\hat{T}_r^{-1}$, and $\hat{L}_f$ in the control of the previous section results in the modified error system

$$\begin{aligned}
\frac{\rm d}{{\rm d}t}\Delta\varphi_r &= -\left[T_r^{-1} + \jmath\omega_g\right]\Delta\varphi_r - \delta T_r^{-1}\varphi_r^{\rm ref} \\
&\quad + \delta R_{\rm req} i_s^{\rm ref} + R_{\rm req}\Delta i_s + v_r
\end{aligned} \tag{27}$$

$$\begin{aligned}
L_f \frac{\rm d}{{\rm d}t}\Delta i_s &= -[R_s + R_{\rm req} + \jmath L_f\omega_s]\Delta i_s + \left[T_r^{-1} - \jmath\omega_r\right]\Delta\varphi_r \\
&\quad + v_s - [\delta R_s + \delta R_{\rm req} + \jmath\delta L_f\omega_s] i_s^{\rm ref} \\
&\quad + \delta T_r^{-1}\varphi_r^{\rm ref} - \delta L_f \frac{\rm d}{{\rm d}t} i_s^{\rm ref}
\end{aligned} \tag{28}$$

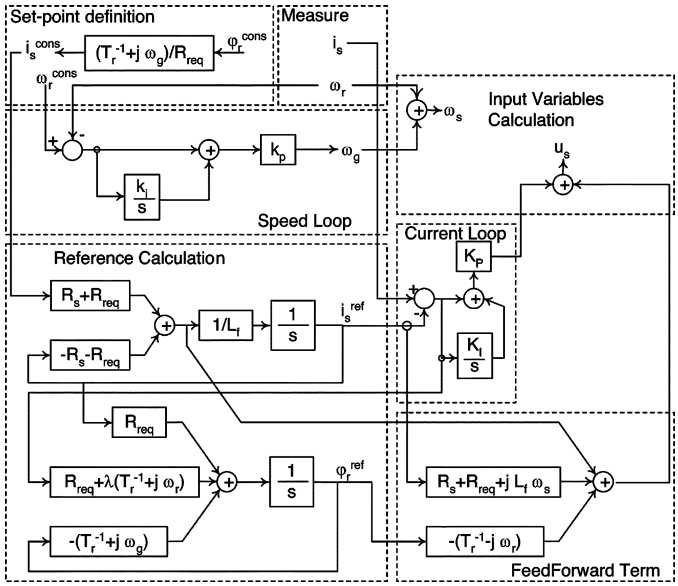

Fig. 1. Block diagram of the proposed controller structure (without adaptation).

where $\delta T_r^{-1} = T_r^{-1} - \hat{T}_r^{-1}$, $\delta R_{\rm req} = R_{\rm req} - \hat{R}_{\rm eq}$, $\delta L_f = L_f - \hat{L}_f$, and $\delta R_s = R_s - \hat{R}_s$.

We propose two adaptation schemes to achieve flux regulation in spite of the parametric uncertainty. The adaptation schemes aim at asymptotically annihilating the parametric (relative) error vector

$$\Delta\theta = \begin{bmatrix} \frac{\delta R_{\rm req}}{R_{\rm req}} \\ \frac{\delta L}{L} \\ \frac{\delta R_s}{R_s} \\ \frac{\delta L_f}{L_f} \end{bmatrix}. \tag{29}$$

A. Time-Scale Separation Approach

Slow adaptation of parameter estimates enforces a time-scale separation between the system dynamics and the adaptation dynamics. This time-scale separation simplifies the design of the adaptation law, which will be based on the steady state of the closed-loop dynamics (24), (28) in the absence of adaptation. The steady state of (27) and (28) is biased by the parametric errors, but it still verifies $\Delta i_s = 0$ because of the integral action (12). Setting the derivatives to zero in (27) and (28) then yields

$$\left[T_r^{-1} + \jmath\omega_g\right]\Delta\varphi_r = \delta R_{\rm req} i_s^{\rm ref} - \delta T_r^{-1}\varphi_r^{\rm ref} \tag{30}$$

$$\begin{aligned}
K_P\eta &= \left[T_r^{-1} - \jmath\omega_r\right]\Delta\varphi_r + \delta T_r^{-1}\varphi_r^{\rm ref} \\
&\quad - [\delta R_s + \delta R_{\rm req} + \jmath\delta L_f\omega_s] i_s^{\rm ref}.
\end{aligned} \tag{31}$$

As a consequence, the design of the parametric adaptation can be based on the steady state of the integral variable η. Using a calculation detailed in theAppendix, (31) can be rewritten as

$$K_P\eta = B^T\Delta\theta + 0\left(\|\,\Delta\theta\,\|^2\right) \tag{32}$$

Authorized licensed use limited to: Rodolphe Sepulchre. Downloaded on May 8, 2009 at 00:30 from IEEE Xplore. Restrictions apply.

where

$$B = \begin{bmatrix} \frac{\omega_s \omega_g}{\hat{T}_r^{-1} + \jmath\omega_g} \varphi_r^{\text{cons}} \\ -\frac{\omega_s \hat{T}_r^{-1}}{\hat{T}_r^{-1} + \jmath\omega_g} \jmath \varphi_r^{\text{cons}} \\ -R_s i_s^{\text{ref}} \\ -\omega_s \jmath L_f i_s^{\text{ref}} \end{bmatrix}. \tag{33}$$

The steady-state relationship (32) provides two algebraic equations in four unknowns. It suggests the adaptation law

$$\frac{\mathrm{d}}{\mathrm{d}t}\Delta\theta = -K_B \overline{B} K_P \eta \tag{34}$$

where $\overline{B}$ denotes the conjugate of B and K_B is a positive definite gain matrix. This adaptation scheme provides the following result.

Theorem 1: Consider the induction motor model (5) and the control law of Section III, where unknown parameters are replaced by their estimates, i.e.,

$$\begin{aligned} u_s =& [\hat{R}_s + \hat{R}_{\text{req}}] i_s^{\text{cons}} + \jmath \hat{L}_f \omega_s i_s^{\text{ref}} \\ & - \left[\hat{T}_r^{-1} - \jmath\omega_r\right] \varphi_r^{\text{ref}} + v_s \qquad (35) \\ \frac{\mathrm{d}}{\mathrm{d}t}\varphi_r^{\text{ref}} =& - \left[\hat{T}_r^{-1} + \jmath\omega_g\right] \varphi_r^{\text{ref}} + \hat{R}_{\text{req}} i_s^{\text{ref}} - v_r \\ \hat{L}_f \frac{\mathrm{d}i_s^{\text{ref}}}{\mathrm{d}t} =& - [\hat{R}_s + \hat{R}_{\text{req}}][i_s^{\text{cons}} - i_s^{\text{ref}}] \\ v_r =& \left[-\hat{R}_{\text{req}} - \lambda\left[\hat{T}_r^{-1} + \jmath\omega_r\right]\right] \Delta i_s \qquad (36) \\ \hat{R}_{\text{req}} i_s^{\text{cons}} =& [\hat{T}_r^{-1} + \jmath\omega_g] \varphi_r^{\text{cons}} \qquad (37) \end{aligned}$$

with the two PI loops for v_s and ω_g determined by (25) and (12), respectively, and with gains $K_P = \varepsilon^{-1}\tilde{K}_P$ and $K_I = \varepsilon^{-1}\tilde{K}_I$. In these expressions, the estimate $\hat{T}_r^{-1}$ stands for $\hat{R}_{\text{req}}/\hat{L}$.

Then, for $\epsilon > 0$ that is small enough, the adaptation law (34) enforces local exponential regulation of the flux and of the mechanical speed for any constant reference $(\varphi^{\text{cons}}, \omega_r^{\text{cons}})$ and any constant load torque τ_L under persistence of excitation of $B = B(t)$, i.e., the existence of positive constants $\alpha > 0$, $\beta > 0$, and $T > 0$ such that

$$\forall t \geq 0 : \alpha I \leq \int_t^{t+T} \overline{B} B^T \mathrm{d}t \leq \beta I. \tag{38}$$

Proof: Choosing large gains $K_P = \varepsilon^{-1}\tilde{K}_P$ and $K_I = \varepsilon^{-1}\tilde{K}_I$ in the control law (25) puts the closed-loop dynamics (27) and (28) in the singularly perturbed form

$$\begin{aligned} \frac{\mathrm{d}}{\mathrm{d}t}\Delta\varphi_r =& - \left[T_r^{-1} + \jmath\omega_g\right] \Delta\varphi_r - \delta T_r^{-1} \varphi_r^{\text{ref}} + \delta R_{\text{req}} i_s^{\text{ref}} \\ & - \left[\hat{R}_{\text{req}} + \lambda\left[\hat{T}_r^{-1} + \jmath\omega_r\right]\right] \Delta i_s \\ \varepsilon L_f \frac{\mathrm{d}}{\mathrm{d}t}\Delta i_s =& - \tilde{K}_P[\Delta i_s + \eta] + \varepsilon B^T \Delta\theta \\ & + O\left(\varepsilon \frac{\mathrm{d}}{\mathrm{d}t}\Delta\varphi_r\right) + O\left(\varepsilon \frac{\mathrm{d}}{\mathrm{d}t} i_s^{\text{ref}}\right) + O(\varepsilon^2) \\ \varepsilon \frac{\mathrm{d}}{\mathrm{d}t}\eta =& \tilde{K}_I \Delta i_s. \end{aligned} \tag{39}$$

For small enough $\varepsilon > 0$, the time-scale separation enforces fast convergence of the solution to an invariant manifold satisfying

$$\begin{cases} \tilde{K}_P \eta = \varepsilon B^T \Delta\theta + O\left(\varepsilon \frac{\mathrm{d}}{\mathrm{d}t}\Delta\varphi_r\right) + O\left(\varepsilon \frac{\mathrm{d}}{\mathrm{d}t} i_s^{\text{ref}}\right) + O(\varepsilon^2) \\ \Delta i_s = O(\varepsilon^2). \end{cases} \tag{40}$$

The reduced dynamics on this slow manifold are the dynamics (16) with the biased set-point relationship (32). In the slow time scale $\tilde{t} = \epsilon t$, and neglecting second-order terms, the adaptation law (34) gives rise to the stable dynamics

$$\tilde{K}_P \frac{\mathrm{d}}{\mathrm{d}\tilde{t}}\Delta\theta = -K_B \overline{B} B^T \Delta\theta. \tag{41}$$

It is well known [23] that exponential stability of the equilibrium $\Delta\theta = 0$ of (41) is equivalent to persistence of excitation of $B = B(t)$.

The time variation of the vector $B = B(t)$ is through the dependence on several state and reference variables, including the mechanical speed ω_r and the piecewise constant reference variable ω_r^{cons}. The interpretation of the persistent excitation condition (38) is further discussed in Section V.

B. Time-Varying Adaptation

We propose a second adaptation scheme that guarantees local exponential stability of the unbiased equilibrium with estimation of the four unknown parameters. The result follows from the approach proposed in [24]. It does not require a time-scale separation, but the order of the controller is augmented by four states with respect to the previous solution.

We introduce two linear filters

$$\begin{aligned} \frac{\mathrm{d}}{\mathrm{d}t}\chi_1 =& - \left[\hat{T}_r^{-1} + \jmath\omega_g\right] \chi_1 - \left(\hat{R}_{\text{eq}} i_s^{\text{ref}} - \hat{T}_r^{-1} \varphi_r^{\text{ref}}\right) \\ \frac{\mathrm{d}}{\mathrm{d}t}\chi_2 =& - \left[\hat{T}_r^{-1} + \jmath\omega_g\right] \chi_2 - \hat{T}_r^{-1} \varphi_r^{\text{ref}}. \end{aligned} \tag{42}$$

Using the change of variables

$$\Delta z = \Delta\varphi_r + \Delta\theta_1 \chi_1 + \Delta\theta_2 \chi_2$$

and restricting the calculations to first-order terms, we compute from (27) and (42)

$$\begin{aligned} \frac{\mathrm{d}}{\mathrm{d}t}\Delta z =& - \left[T_r^{-1} + \jmath\omega_g\right] \Delta z + R_{\text{req}} \Delta i_s \\ & + v_r + \chi_1 \frac{\mathrm{d}}{\mathrm{d}t}\Delta\theta_1 + \chi_2 \frac{\mathrm{d}}{\mathrm{d}t}\Delta\theta_2. \end{aligned}$$

The control law

$$v_r = -\hat{R}_{\text{eq}} \Delta i_s - \lambda\left[\hat{T}_r^{-1} + \jmath\omega_r\right] \Delta i_s - \chi_1 \frac{\mathrm{d}}{\mathrm{d}t}\Delta\theta_1 - \chi_2 \frac{\mathrm{d}}{\mathrm{d}t}\Delta\theta_2 \tag{43}$$

corresponds to the sum of (36) and the additional signal $-\chi_1(\mathrm{d}/\mathrm{d}t)\Delta\theta_1 - \chi_2(\mathrm{d}/\mathrm{d}t)\Delta\theta_2$, which will be determined by the adaptation law. Neglecting again higher order terms, the control law (43) yields the closed-loop system

$$\frac{\mathrm{d}}{\mathrm{d}t}\Delta z = - \left[T_r^{-1} + \jmath\omega_g\right] \Delta z - \lambda\left[T_r^{-1} + \jmath\omega_r\right] \Delta i_s \tag{44}$$

Authorized licensed use limited to: Rodolphe Sepulchre. Downloaded on May 8, 2009 at 00:30 from IEEE Xplore. Restrictions apply.

$$L_f \frac{\mathrm{d}}{\mathrm{d}t}\Delta i_s = \left[T_r^{-1} - \jmath\omega_r\right]\Delta z - [R_s + R_{\mathrm{req}} + \jmath L_f \omega_s]\Delta i_s + W^T \Delta\theta + v_s \quad (45)$$

where

$$W = -\begin{bmatrix} \left[\hat{T}_r^{-1} - \jmath\omega_r\right]\chi_1 + \hat{R}_{\mathrm{eq}} i_s^{\mathrm{ref}} - \hat{T}_r^{-1}\varphi_r^{\mathrm{ref}} \\ \left[\hat{T}_r^{-1} - \jmath\omega_r\right]\chi_2 + \hat{T}_r^{-1}\varphi_r^{\mathrm{ref}} \\ \hat{R}_s i_s^{\mathrm{ref}} \\ \jmath\omega_s \hat{L}_f i_s^{\mathrm{ref}} \end{bmatrix}. \quad (46)$$

Note that, in steady state, the vector W in (46) is equal to the vector B in (33). The proposed adaptation dynamics is given by

$$\frac{\mathrm{d}}{\mathrm{d}t}\Delta\theta = -K_W \overline{W} L_f \Delta i_s \quad (47)$$

with $K_W > 0$ being a positive definite gain matrix, which enforces exponential convergence of Δz and Δi_s to zero, as shown with the Lyapunov function

$$V(\Delta z, \Delta i_s, \Delta\theta, \eta) = \frac{1}{2}|\Delta z|^2 + \frac{\lambda L_f}{2}|\Delta i_s|^2 + \frac{\lambda}{2}(\Delta\theta)^T K_W^{-1}\Delta\theta + \frac{\lambda}{2K_I}|\eta|^2 \quad (48)$$

whose time-derivative satisfies

$$\dot{V}(\Delta z, \Delta i_s, \Delta\theta) = -T_r^{-1}|\Delta z|^2 - \lambda[R_s + R_{\mathrm{req}} + K_P]|\Delta i_s|^2. \quad (49)$$

Theorem 2: Consider the induction motor model (5) and the control law

$$\begin{aligned} u_s &= [\hat{R}_s + \hat{R}_{\mathrm{req}}] i_s^{\mathrm{cons}} + \jmath \hat{L}_f \omega_s i_s^{\mathrm{ref}} - \left[\hat{T}_r^{-1} - \jmath\omega_r\right]\varphi_r^{\mathrm{ref}} + v_s \\ \frac{\mathrm{d}}{\mathrm{d}t}\varphi_r^{\mathrm{ref}} &= -\left[\hat{T}_r^{-1} + \jmath[\omega_s - \omega_r]\right]\varphi_r^{\mathrm{ref}} + \hat{R}_{\mathrm{req}} i_s^{\mathrm{ref}} - v_r \\ \hat{L}_f \frac{\mathrm{d}i_s^{\mathrm{ref}}}{\mathrm{d}t} &= -[\hat{R}_s + \hat{R}_{\mathrm{req}}]\left[i_s^{\mathrm{cons}} - i_s^{\mathrm{ref}}\right] \\ v_r &= -\hat{R}_{\mathrm{eq}}\Delta i_s - \lambda\left[\hat{T}_r^{-1} + \jmath\omega_r\right]\Delta i_s - \chi_1 \frac{\mathrm{d}}{\mathrm{d}t}\Delta\theta_1 - \chi_2 \frac{\mathrm{d}}{\mathrm{d}t}\Delta\theta_2 \end{aligned}$$

and the two PI loops for v_s and ω_s determined by (25) and (12). In these expressions, the estimate $\hat{T}_r^{-1}$ stands for $\hat{R}_{\mathrm{req}}/\hat{L}$.

Then, the adaptation law defined by (42) and (47) enforces (local) exponential regulation of the flux and of the mechanical speed for any constant reference $(\varphi^{\mathrm{cons}}, \omega_r^{\mathrm{cons}})$ and any constant load torque τ_L under persistence of excitation of the vector (46). Note that the definition of v_r in (43) uses signals $\mathrm{d}/\mathrm{d}t\Delta\theta_1$ and $\mathrm{d}/\mathrm{d}t\Delta\theta_2$, which are obtained from (47).

Proof: We prove exponential convergence of the equilibrium $\Delta x = (\Delta z, \Delta i_s, \Delta\theta, \eta) = 0$ of the linear time-varying system (44), (45), (47) with the PI loop (25). The Lyapunov function (48) and its time derivative (49) show that the equilibrium is Lyapunov stable and that the "output" signal $\Delta y(t) = (\Delta z(t), \Delta i_s(t))$ is in $L_2(t_0, \infty)$ for every initial condition in a neighborhood of the equilibrium and any initial time t_0. Exponential stability of $\Delta x = 0$ is then easily shown to be equivalent to uniform observability of the system with output $\Delta y = (\Delta z, \Delta i_s)$ (see, e.g., [23] or [25]). Observe that the system dynamics (44), (45), (47), and (25) decompose as

$$\frac{\mathrm{d}}{\mathrm{d}t}\Delta x = K(t)\begin{bmatrix}\Delta z \\ \Delta i_s\end{bmatrix} + \begin{bmatrix} 0 \\ L_f^{-1} W^T \\ 0 \end{bmatrix}\Delta\theta \quad (50)$$

where the matrix $K(t)$ is easily identified from (44), (45), and (47) and is uniformly bounded (in L_2 norm) over any finite time interval. Expression (50) shows that the closed-loop system is equivalent under the bounded output injection $-K(t)\Delta y$ to

$$\frac{\mathrm{d}}{\mathrm{d}t}\Delta x = \begin{bmatrix} 0 \\ L_f^{-1} W^T \\ 0 \end{bmatrix}\Delta\theta.$$

Uniform observability of the latter system is equivalent to persistence of excitation of $W(t)$. Because uniform observability is invariant under bounded output injection, one concludes that the closed-loop dynamics (50) is also uniformly observable, which concludes the proof.

Although not considered in this paper, projection algorithms may be suitable to restrict the admissible range of parameter estimates on the basis of physical considerations [6], [8].

V. Parametric Sensitivity Analysis

A. Parametric Sensitivity of the Adaptation

For fixed values of ω_s and ω_g, the null space of B is at least of dimension two so that at most two linearly independent combinations of the parameters can be adapted at a given operating point determined by $(\omega_r^{\mathrm{cons}}, \tau_L)$. These combinations are determined by the 2-D dominant eigensubspace of the matrix $\bar{B}B^T$. The location of this dominant eigensubspace largely varies according to the operating condition of the motor. This variation can be inferred from Fig. 2, which represents the variation (in modulus) of each element of the normalized vector$B/\parallel B \parallel$ across the plane$(\omega_r^{\mathrm{cons}}, \tau_L)$ of operating conditions. Because the largest two elements of the vector are well separated from the smallest two (in modulus), they provide a close approximation of the dominant eigensubspace. Fig. 2 therefore provides the following qualitative conclusions.

1) The sensitivity of the adaptation to the rotor resistance (parameter R_{req}) is high across the entire region of operating conditions except when $|T_r\omega_s|$ or $|T_r\omega_g|$ is small, i.e., at low speed and at low load torque.
2) The sensitivity of the adaptation to the inductance L is high across the entire region of operating conditions except when $|T_r\omega_s|$ is small, i.e., at low speed.
3) The sensitivity of the adaptation to the stator resistance R_s is low across the entire region of operating conditions except when $|T_r\omega_s|$ is small, i.e., at low speed.
4) The sensitivity of the adaptation to the leakage inductance L_f is low across the entire region of operating conditions except when $|T_r\omega_s|$ and $|T_r\omega_g|$ are large, i.e., at high load torque and sufficient speed.

Authorized licensed use limited to: Rodolphe Sepulchre. Downloaded on May 8, 2009 at 00:30 from IEEE Xplore. Restrictions apply.

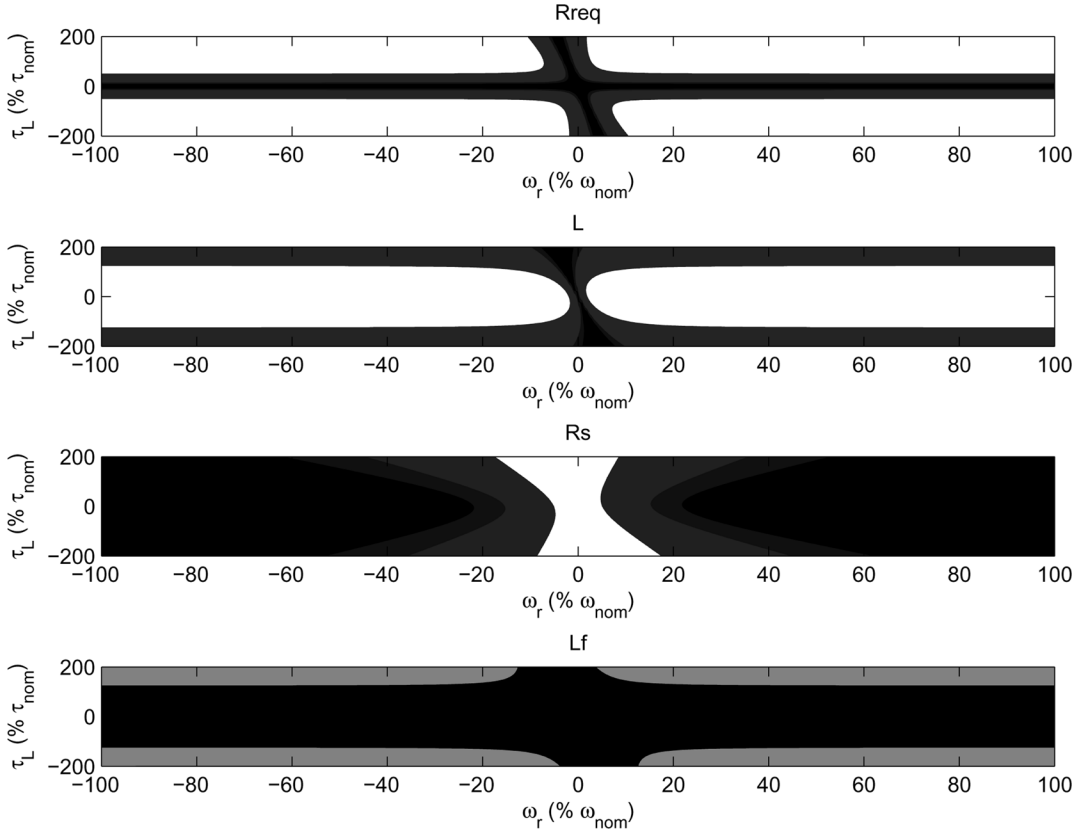

Fig. 2. Relative sensitivity of the adaptation to each parameter is measured by variation of the modulus of each coefficient of the normalized vector $B/\parallel B \parallel$ across the plane of operating conditions. The white color stands for a modulus larger than 0.75, whereas the black color stands for a modulus smaller than 0.1.

This sensitivity analysis thus reveals that the different parameters can be estimated in different operating conditions. For most operating conditions of the motor, the adaptation of $R_{\rm req}$ and L largely dominates the adaptation of R_s and L_f. Nevertheless, the estimation of the parameter R_s is efficient at low speed, and the estimation of the parameter L_f is efficient at high load torque (and sufficient speed).

B. Parametric Sensitivity of the (Static) Closed-Loop Performance

Even in the absence of parametric estimation, the integral action of the controller of Section II achieves speed and current regulation. In contrast, the asymptotic flux is biased by the parametric uncertainties δR_{req} and δL, as shown by static (30). The following two performance criteria further motivate the estimation of $R_{\rm req}$ and L.

1) Torque estimation: The steady state of mechanical (1) provides an estimation of the load torque τ_L

$$\tau_L = \frac{3n_p}{2}\langle i_s, \jmath\varphi_r\rangle. \tag{51}$$

Current regulation to $i_s^{\rm cons} = \hat{T}_r^{-1} + j\omega_g/\hat{R}_{\rm req}\varphi_r^{\rm cons}$ results in the load torque estimation

$$\tau_L = \frac{3n_p}{2}\left\langle \frac{\hat{T}_r^{-1} + j\omega_g}{\hat{R}_{\rm req}}\varphi_r^{\rm cons}, \jmath\varphi_r \right\rangle \tag{52}$$

which is biased only by the parametric errors on $R_{\rm req}$ and $L = T_r^{-1}/R_{\rm req}$ but not biased by the parametric errors on R_s and L_f.

TABLE II
PARAMETERS OF THE CONTROLLER

Parameter	*notation*	*numerical value used in paper*
velocity loop (prop. gain)	k_p	1.4
velocity loop (int. gain)	k_i	15.7
current loop (prop. gain)	K_p	7.0
current loop (int. gain)	K_I	790

2) Current consumption: Current consumption can be optimized when the current reference is unbiased, which again requires accurate estimation of the parameters $R_{\rm req}$ and L but does not require accurate estimation of the parameters R_s and L_f.

We thus conclude that the static performance of the motor in closed-loop operation is determined by the parameters $R_{\rm req}$ and L but is independent of the parameters R_s and L_f.

C. Simulation Results

The simulations in this section illustrate the closed-loop behavior obtained with the proposed adaptive controller and the performance improvement provided by the parameter adaptation. We use the numerical values in Table I for the motor model and the numerical values in Table II for the controller parameters.

The control gain λ in (22) is chosen as

$$\lambda = \frac{R_{\rm req}}{L_f}\sqrt{T_r^{-2} + \omega_r^2}.$$

Authorized licensed use limited to: Rodolphe Sepulchre. Downloaded on May 8, 2009 at 00:30 from IEEE Xplore. Restrictions apply.

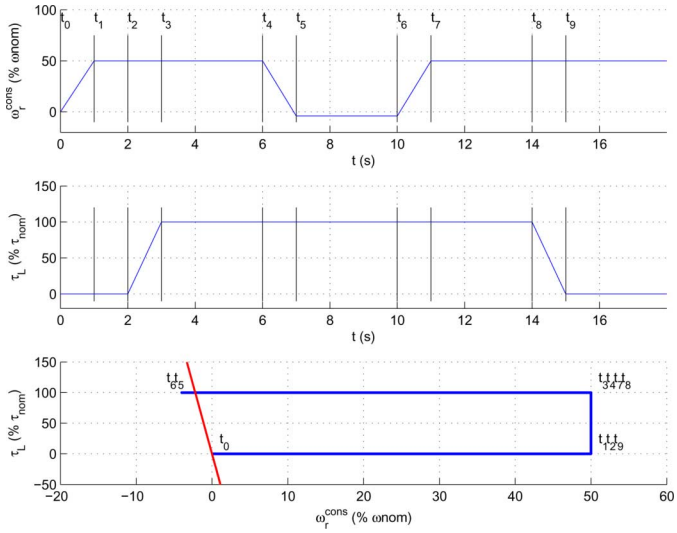

Fig. 3. Time history and phase portrait of the desired speed $\omega_r^{\rm cons}$ and load torque τ_L used for the simulation and experimental results.

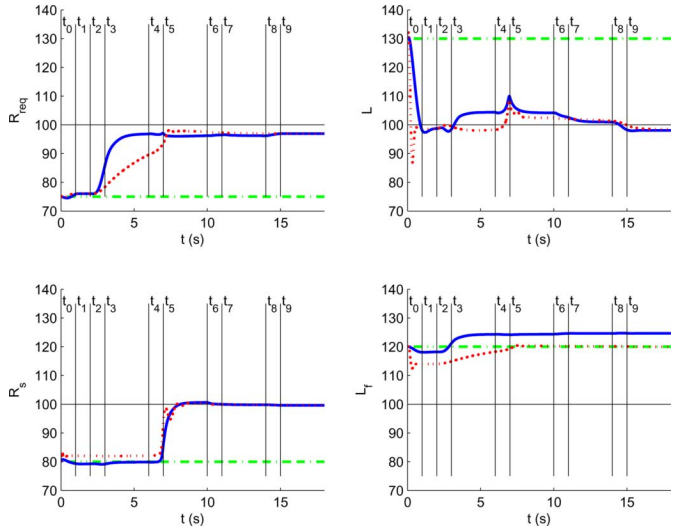

Fig. 4. Simulated online adaptation of the four parameters along the reference trajectory shown in Fig. 3. (Dashed) Initial estimate. (Dotted) Adaptation with the time-varying scheme. (Solid) Adaptation with the time-scale scheme. The scale is in percentage of the (constant) true parameter value.

For the two proposed adaptation schemes, the gain in (34) is chosen as

$$\frac{2T_r^{-1}}{3\|B\|^2}$$

while the gain in (47) is chosen as

$$\frac{(36\pi)^2}{\|W\|^2}.$$

(Note the state-dependent scaling of the gains, whereas the Lyapunov functions used in the convergence analysis require constant gains). We first consider a reference trajectory for ω_r and τ_L shown in Fig. 3. The reference trajectory is also plotted in the $(\omega_r^{\rm cons}, \tau_L)$ plane to illustrate that regions with different relative parametric sensitivity of the adaptation are visited. Fig. 4 shows

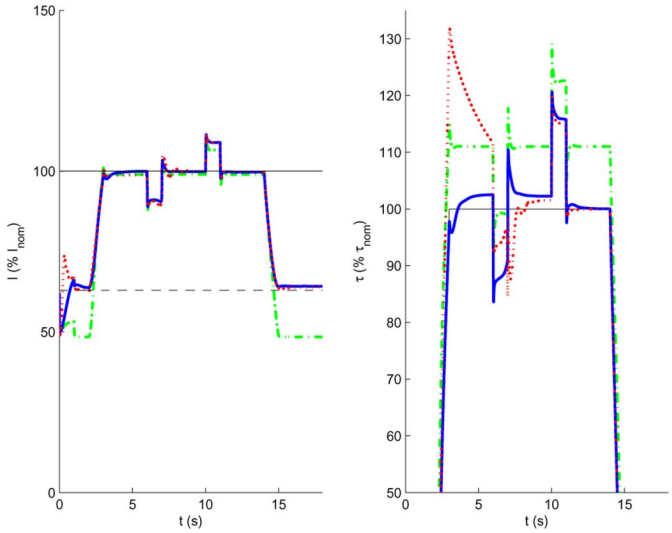

Fig. 5. Simulated online estimation of load torque and consumed current along the reference trajectory shown in Fig. 3. (Dashed) Without adaptation. (Dotted) With adaptation (time-varying scheme). (Solid) With adaptation (time-scale scheme). The scale is in percentage of the (constant) true parameter value.

the time evolution of the four parameters, with initial errors of more than 20% on each parameter. It is seen that the convergence of the parameters closely follows the prediction of Fig. 2. The operation at high speed and low load torque (from time t_0 to time t_2) results in fast adaptation of the parameter L only.

The load torque is increased from time t_2, allowing for the simultaneous adaptation of L and $R_{\rm req}$. From time t_5, low-speed operation of the motor allows for the adaptation of R_s. The adaptation of L_f is poor throughout the simulation. Fig. 5 shows the estimated load torque and the estimated current consumption, showing the benefit of the adaptation with respect to a controller scheme without adaptation. Due to the natural time-scale separation between the electrical and mechanical variables, the simulation shows no significant difference between the two adaptation schemes discussed in Section IV.

As a second illustration, we consider operation of the motor at a constant operating point but with a slow drift of resistances. In reality, the thermal drift would be even slower but comparable in amplitude. Figs. 6 and 7 show how the parametric adaptation allows one to compensate for the corresponding drift in load torque estimation and current consumption.

VI. Simplified Adaptation Scheme and Experimental Results

A. Simplified Adaptation Scheme

The discussion in the previous section has shown that the parametric sensitivity of the closed-loop performance matches the parametric sensitivity of the proposed adaptation scheme in most operating conditions, i.e., away from the thin-shaded region in Fig. 2(a) and (b).

This motivates a reduced adaptation scheme in which only the parameters $R_{\rm req}$ and L are adapted according to (34) or (47). This corresponds to an adaptation gain

$$K_B = \frac{1}{\|B\|^2}\mathrm{diag}\{1, 1, \epsilon, \epsilon\}$$

Authorized licensed use limited to: Rodolphe Sepulchre. Downloaded on May 8, 2009 at 00:30 from IEEE Xplore. Restrictions apply.

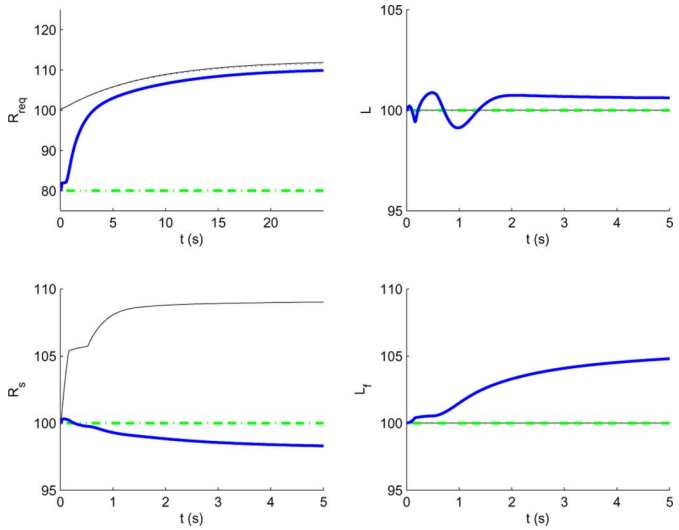

Fig. 6. Simulated online adaptation of the four parameters at the fixed operating point $(\omega_r^{\text{cons}}, \tau_L) = (50\%, 50\%)$ to track (slow) variations of the parameters.

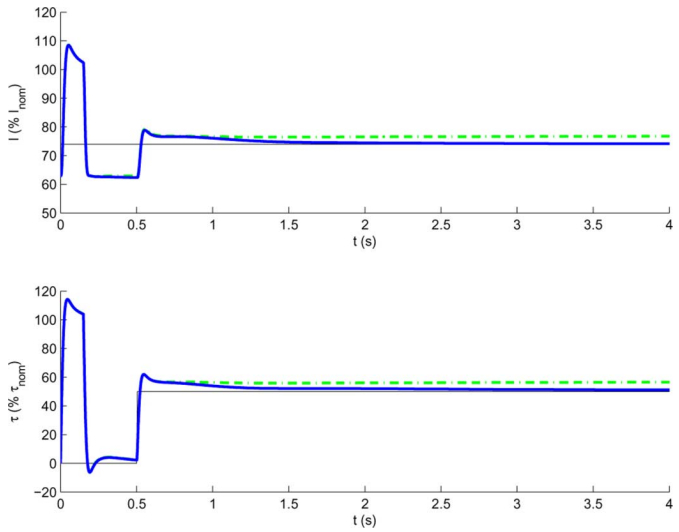

Fig. 7. Simulated online estimation of load torque and consumed current at the fixed operating point $(\omega_r^{\text{cons}}, \tau_L) = (50\%, 50\%)$ during (slow) variations of the parameters.

in the limit for $\epsilon > 0$ tending to zero. In the limit, the parameters R_s and L_f are no longer adapted. The adaptation gain on the two other parameters is kept constant, except in the region of poor sensitivity, which we define as

$$|T_r\omega_s| \leq \epsilon_0 \text{ or } |T_r\omega_g| \leq \epsilon_1. \tag{53}$$

In that region, the adaptation is simply turned off. For the results presented hereinafter, we choose $\epsilon_0 = 4$ and $\epsilon_1 = 1/4$. The block diagram in Fig. 8 shows the addition of the adaptation scheme within the complete block diagram of the controller. In this figure, the dead zone of the adaptation gain specified by (53) is represented by the nonlinear gain $\gamma(\omega_s, \omega_g)$.

The simulations in Figs. 9–11 illustrate the closed-loop behavior of the motor for the same scenario as in Figs. 4 and 5. The static resistance parameter R_s is no longer adapted, but the figure shows the little impact of the simplified adaptation

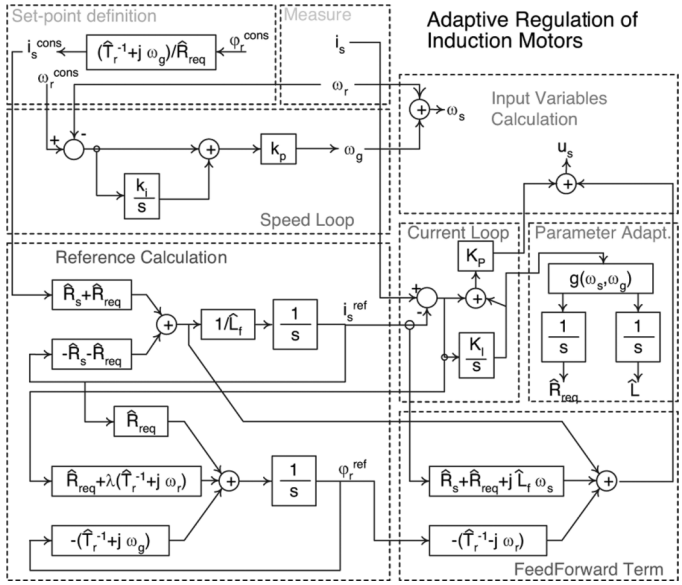

Fig. 8. Block diagram representation of the complete controller with the reduced adaptation included.

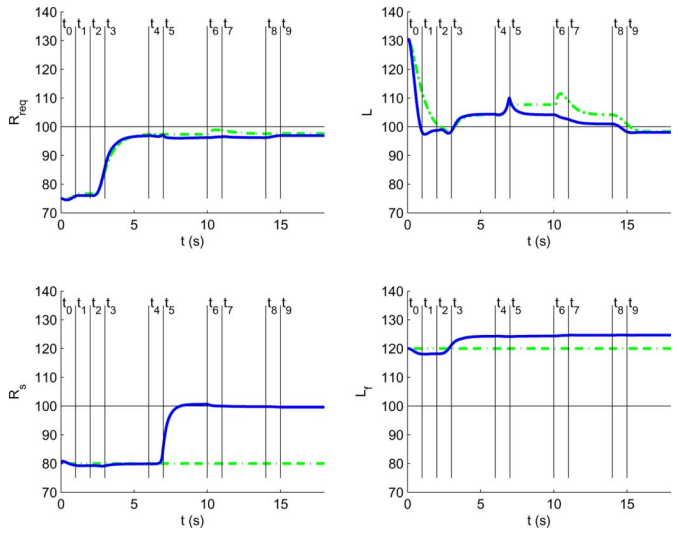

Fig. 9. Same simulation as in Fig. 4 with the (full curve) full adaptation scheme based on time-scale separation and with the (dashed curve) reduced adaptation scheme.

scheme on the estimated load torque and current with respect to the full adaptation scheme of Section IV.

It should be emphasized that limiting the adaptation to only two parameters prevents the convergence of *all* the estimated parameters to true values. The performance of the reduced adaptation scheme is nevertheless similar to the performance of the full adaptation scheme because of the poor sensitivity of the latter to two of the parameters. Simulations suggest that adaptation of the two parameters R_{req} and L is sufficient to achieve correct flux orientation as well as accurate estimation of the load torque and of the consumed current.

B. Experimental Results

The algorithm has been implemented on an industrial variable-speed-drive product, with a range of motor power ratings

Authorized licensed use limited to: Rodolphe Sepulchre. Downloaded on May 8, 2009 at 00:30 from IEEE Xplore. Restrictions apply.

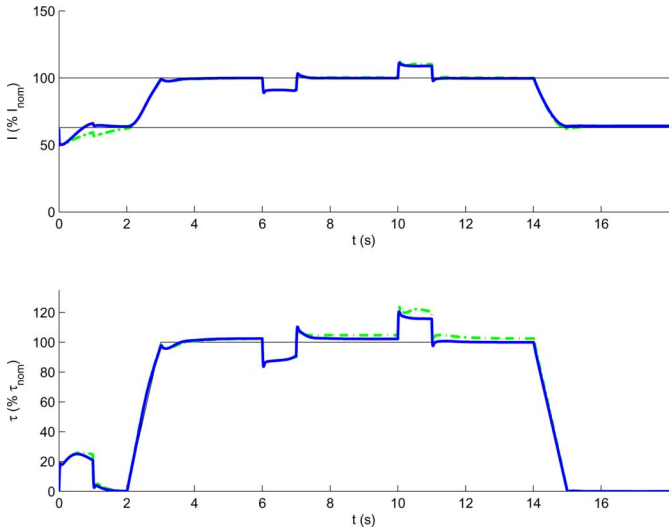

Fig. 10. Same simulation as in Fig. 5 with the (full curve) full adaptation scheme based on time-scale separation and with the (dashed curve) reduced adaptation scheme.

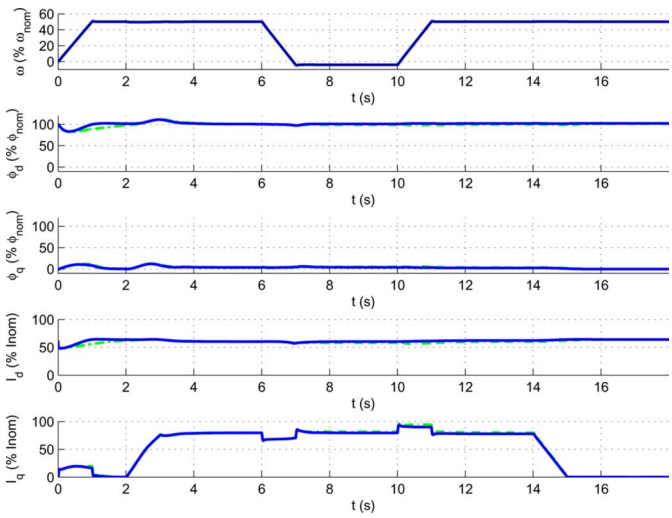

Fig. 11. Time history of the five motor state variables for the simulation in Fig. 5 with the (full curve) full adaptation scheme based on time-scale separation and with the (dashed curve) reduced adaptation scheme. The reference trajectories (almost superposed to the full curves) are in dotted.

between 0.37 and 75 kW. The experimental tests have been carried out using a 4-kW 400-V three-phase drive, as shown in Fig. 12. The test bench consists of the following.

1) 4-kW induction machine. Its nameplate gives the motor data (415 V, 7.9 A, 1445 r/min, and 50 Hz).
2) This standard induction motor is driven by our industrial product.
3) An 11-kW dc machine is used to provide the load torque. It is driven by an industrial dc drive. We control the load torque application and the load torque value by a logical input and an analog input.

The microcontroller dedicated to the control algorithm is a 32-b microcontroller with an internal ROM size of 128 kB and an internal RAM size of 6 kB. The maximum operating frequency is 40 MHz. We used directly the HMI of the industrial product to

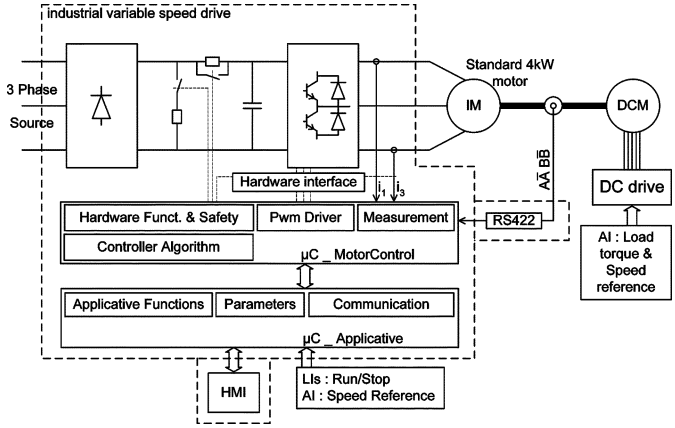

Fig. 12. Block diagram of the experimental setup.

experiment our algorithm by configuring the closed-loop control law. Logical inputs are used to start and stop the drive. An analog input is used to select the set-point speed. To obtain the speed information, we use an encoder interface board with RS422-compatible differential outputs. The number of encoder pulses is 1024. This option encoder board is plugged on the industrial variable-speed drive. The pulsewidth-modulation (PWM) switching frequency used for these tests is 4 kHz. The PWM method used for these experimental tests is a standard three-phase sinusoidal PWM in the illustrated speed area. The currents and the dc voltage are synchronously measured with a sampling period of 250 μs. Only two phase currents are measured using shunts. A computer is linked to the industrial variable-speed drive to collect the data calculated or measured by the drive. The standard Modbus communication protocol integrated in the drive is used.

We present two experimental results that parallel the two simulation results presented in the previous section. We first consider the same scenario as in Section IV (see Fig. 3). Figs. 13 and 14 show the time evolution of the two estimated parameters and of the load torque estimation. As in the simulation, the parametric adaptation provides a clear improvement over the no-adaptive-control scheme for the load torque and current estimation.

As a second experiment, we consider operation of the motor at a constant operating point over a time horizon that causes thermal drift of the parameters. Figs. 15 and 16 show how the parametric adaptation allows one to compensate for the corresponding drift in load torque estimation and current consumption.

VII. Conclusion

This paper has proposed an adaptive controller that locally achieves robust regulation of speed and flux in an induction motor with online estimation of all the electrical parameters. A sensitivity analysis has shown that only two of the four electrical parameters determine the static closed-loop performance and that these two parameters are those that can be precisely estimated in most operating conditions, i.e., away from (very) low-speed and (very) low-load torque regimes. The proposed adaptive controller consists of four states that generate reference

Authorized licensed use limited to: Rodolphe Sepulchre. Downloaded on May 8, 2009 at 00:30 from IEEE Xplore. Restrictions apply.

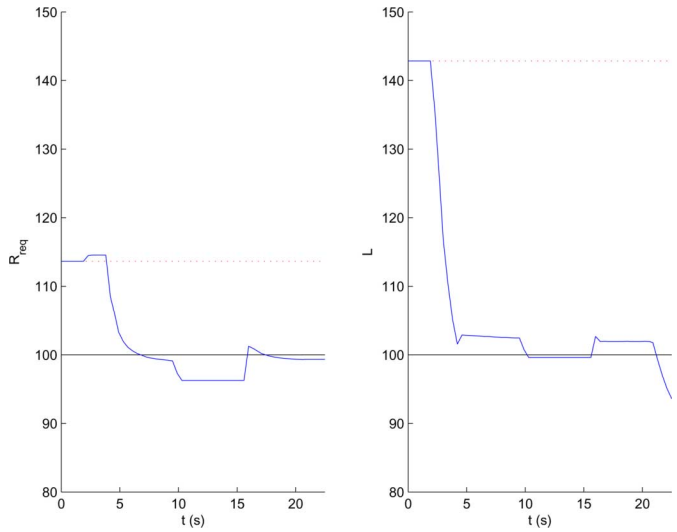

Fig. 13. Online parametric adaptation during an experiment mimicking the reference trajectory shown in Fig. 3.

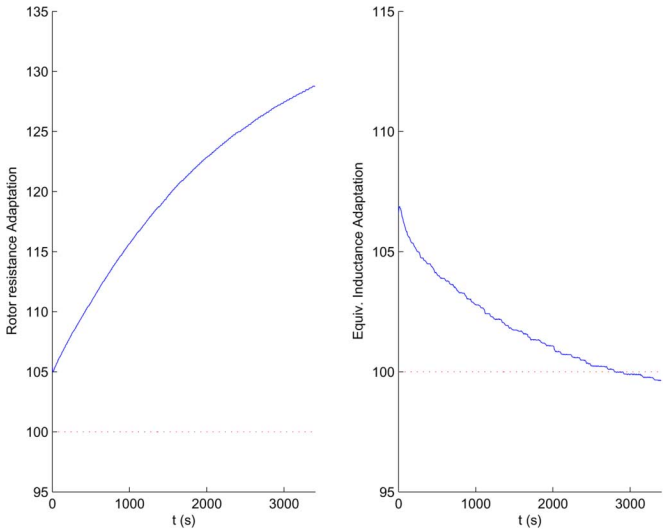

Fig. 15. Online parametric adaptation during an experiment at the fixed operating point $(\omega_r^{\text{cons}}, \tau_L^*) = (50\%, 100\%)$ to track (thermal) variations of the parameters.

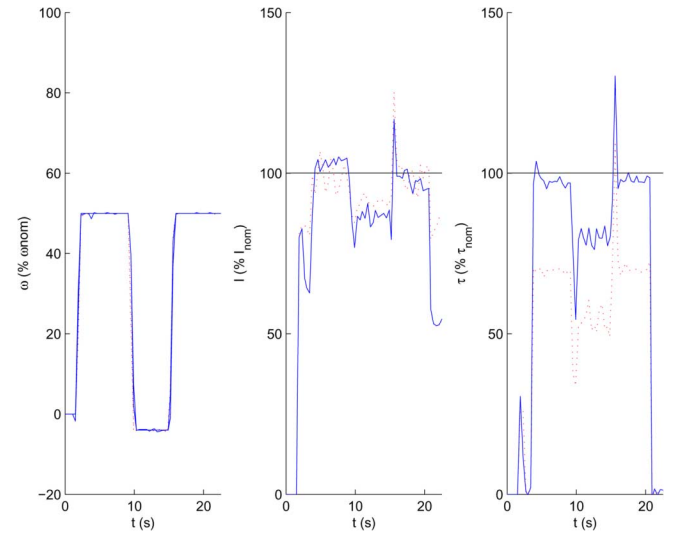

Fig. 14. Evolution of mechanical speed (measured) and online estimation of load torque and consumed current during the experiment shown in Fig. 13. The dotted curves correspond to an experiment with the same control algorithm without adaptation.

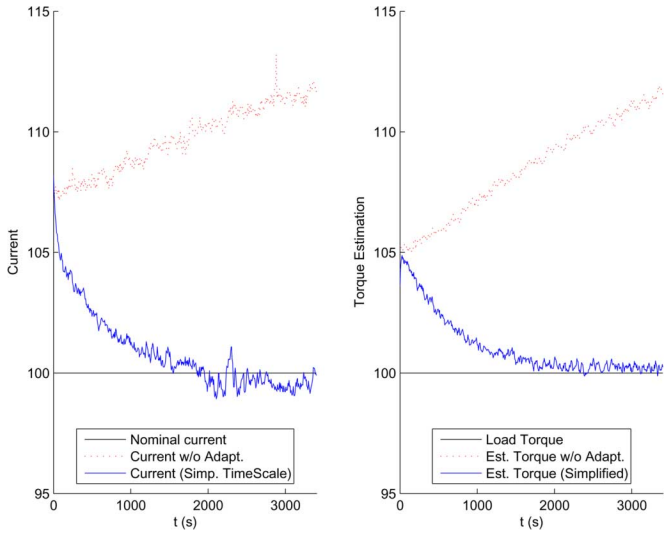

Fig. 16. Online estimation of load torque and consumed current during the same experiment as in Fig. 15. The dotted curve provides the corresponding estimation without the parameter adaptation.

trajectories for the electrical variables, three states that achieve integral action on the mechanical speed and current variables, and two estimates of parameters. The (moderate) cost of two extra states for the parametric adaptation allows one for online accurate estimation of the load torque and current consumption. The results of this paper have been illustrated both by simulation and by experimental validation on an industrial product. An important issue for further research is to accommodate the proposed controller design with the current and voltage physical limitations imposed by the operation of the machine in a real industrial application.

APPENDIX

Summing (30) and (31) yields

$$K_P \eta = -\jmath \omega_s \Delta\varphi_r - \delta R_s i_s^{\text{ref}} - \jmath \delta L_f \omega_s i_s^{\text{ref}}. \tag{54}$$

Restricting calculations to first-order terms in the errors yields the identities

$$\begin{aligned}\delta T_r^{-1} &= \delta\left(\frac{R_{\text{req}}}{L}\right) = \frac{\delta R_{\text{req}}}{L} - T_r^{-1}\frac{\delta L}{L} \\ &= T_r^{-1}\left(\frac{\delta R_{\text{req}}}{R_{\text{req}}} - \frac{\delta L}{L}\right)\end{aligned}$$

and therefore

$$\begin{aligned}\left[T_r^{-1} + \jmath\omega_g\right]\Delta\varphi_r &= \delta R_{\text{req}} i_s^{\text{ref}} - \delta T_r^{-1}\varphi_r^{\text{ref}} \\ &= \jmath\omega_g \varphi_r^{\text{cons}} \frac{\delta R_{\text{req}}}{R_{\text{req}}} + T_r^{-1}\varphi_r^{\text{cons}}\frac{\delta L}{L}.\end{aligned} \tag{55}$$

Notice that having φ_r^{cons} instead of φ_r^{ref} on the right-hand side of (55) corresponds to neglecting a second-order error term. Ex-

Authorized licensed use limited to: Rodolphe Sepulchre. Downloaded on May 8, 2009 at 00:30 from IEEE Xplore. Restrictions apply.

pression (32) is obtained by substituting (55) in the steady-state relationship (54).

ACKNOWLEDGMENT

This paper presents research results of the Belgian Network Dynamical Systems, Control, and Optimization (DYSCO), supported by the Interuniversity Attraction Poles Programme, which is initiated by the Belgian State, Science Policy Office. The scientific responsibility rests with its authors. The original manuscript was completed while J. Moreno-Valenzuela was a Postdoctoral Researcher with the Université de Liège.

REFERENCES

[1] F. Blaschke, "The principle of field orientation applied to the new transvector closed-loop control system for rotating field machines," *Siemens-Rev.*, vol. 39, pp. 217–220, 1972.
[2] W. Leonhard, *Control of Electrical Drives*. New York: Springer-Verlag, 1985.
[3] D. Dawson, J. Hu, and T. Burg, *Nonlinear Control of Electric Machinery*. New York: Marcel Dekker, 1998.
[4] P. Vas, *Artificial Intelligence-Based Electrical Machines and Drives*. Oxford, U.K.: Oxford Press, 1999.
[5] A. Trzynadlowski, *The Field Orientation Principle in Control of Induction Motors*. Norwell, MA: Kluwer, 1994.
[6] R. Marino and P. Tomei, *Nonlinear Control Design—Geometric, Adaptive and Robust*. Englewood Cliffs, NJ: Prentice-Hall, 1976.
[7] A. Isidori, *Nonlinear Control Systems*, 3rd ed. Berlin, Germany: Springer-Verlag, 1995.
[8] M. Krstić, I. Kanellakopoulos, and P. Kokotović, *Nonlinear and Adaptive Control Design*. New York: Wiley, 1995.
[9] R. Sepulchre, M. Jankovic, and P. Kokotović, *Constructive Nonlinear Control*. New York: Springer-Verlag, 1997.
[10] A. J. Van der Schaft, *$\mathcal{L}_2$-Gain and Passivity Techniques in Nonlinear Control*. London, U.K.: Springer-Verlag, 2000.
[11] R. Ortega, A. Loria, P. Nicklasson, and H. Sira-Ramirez, *Passivity-Based Control of Euler–Lagrange Systems*. New York: Spinger-Verlag, 1998.
[12] G. Espinosa and R. Ortega, "State observers are unnecessary for induction motor control," *Syst. Control Lett.*, vol. 23, no. 5, pp. 315–323, Nov. 1994.
[13] G. Espinosa and R. Ortega, "An output feedback globally stable controller for induction motor control," *IEEE Trans. Autom. Control*, vol. 40, no. 1, pp. 138–143, Jan. 1995.
[14] P. Nicklasson, R. Ortega, and G. Espinosa, "Passivity-based control of a class of Blondel–Park transformable electric machines," *IEEE Trans. Autom. Control*, vol. 42, no. 5, pp. 629–647, May 1997.
[15] K. Kim, R. Ortega, A. Charara, and J. Vilain, "Theoretical and experimental comparison of two nonlinear controllers for current-fed induction motors," *IEEE Trans. Control Syst. Technol.*, vol. 5, no. 3, pp. 338–348, May 1997.
[16] S. Peresada, A. Tilli, and A. Tonielli, "Theoretical and experimental comparison of indirect field-oriented controllers for induction motors," *IEEE Trans. Power Electron.*, vol. 18, no. 1, pp. 151–163, Jan. 2003.
[17] A. Behal, M. Feemster, and D. Dawson, "An improved indirect field-oriented controller for the induction motor," *IEEE Trans. Control Syst. Technol.*, vol. 11, no. 2, pp. 248–252, Mar. 2003.
[18] J. Stephan, M. Bodson, and J. Chiasson, "Real-time estimation of the parameters and fluxes of induction motors," *IEEE Trans. Ind. Appl.*, vol. 30, no. 3, pp. 746–759, May/Jun. 1994.
[19] C. Chang and H. Wang, "An efficient method for rotor resistance identification for high-performance induction motor vector control," *IEEE Trans. Ind. Electron.*, vol. 37, no. 6, pp. 477–482, Dec. 1990.
[20] R. Marino, S. Peresada, and P. Tomei, "On-line stator and rotor resistance estimation for induction motors," *IEEE Trans. Control Syst. Technol.*, vol. 8, no. 3, pp. 570–579, May 2000.
[21] R. Marino, S. Peresada, and P. Tomei, "Global adaptive output feedback control of induction motors with uncertain rotor resistance," *IEEE Trans. Autom. Control*, vol. 44, no. 5, pp. 967–983, May 1999.
[22] R. Ortega, P. Nicklasson, and G. Espinosa, "On speed control of induction motors," *Automatica*, vol. 32, no. 3, pp. 455–460, Mar. 1996.
[23] B. D. Anderson, "Exponential stability of linear equations arising in adaptive identification," *IEEE Trans. Autom. Control*, vol. AC-22, no. 1, pp. 84–88, Feb. 1977.
[24] Q. Zhang, "Adaptive observer for multiple-input–multiple-output (MIMO) linear time-varying systems," *IEEE Trans. Autom. Control*, vol. 47, no. 3, pp. 525–529, Mar. 2002.
[25] D. Aeyels, R. Sepulchre, and J. Peuteman, "Asymptotic stability conditions for time-variant systems and observability: Uniform and non-uniform criteria," *Math. Control, Signals, Syst.*, no. 11, pp. 1–27, 1998.

Fabrice Jadot received the Engineering degree in applied mathematics from the Université Catholique de Louvain, Louvain-la-Neuve, Belgium, in 1992, and the Ph.D. degree in automatic control from the Center of Engineering Systems, Automatics and Applied Mechanics, Université Catholique de Louvain, in 1996.

Then, he was with Schneider Electric SA in 1997 as a Motor Control Engineer. In 2000, he was appointed as Leader of the Motor Control Group, Schneider Toshiba Inverter Europe (STIE), Pacy-sur-Eure, France, where he is currently the Vice President of R&D. He was the head of R&D inside STIE in 2004 and took other technical functions in 2005. He has contributed to the publication of a few papers as well as to the deposit of patents. His fields of interest include innovation in variable-speed drives like, e.g., robust motor control.

Francois Malrait received the Diploma of Engineer from the Ecole Supérieure d'Electricité (Gif-sur-Yvette), Paris, France, in 1995 and the Ph.D. degree in automatica and applied mathematics from the Centre Automatique et Systèmes of l'Ecole des Mines de Paris, Paris, in 2001.

He is currently the Head of the Motor Control Team, Schneider Toshiba Inverter Europe, Pacy-sur-Eure, France. His fields of interest include identification and nonlinear control of electrical machines.

Javier Moreno-Valenzuela received the B.Sc. degree in electronics engineering from the Instituto Tecnológico de Culiacán, Culiacán, Mexico, in 1997 and the Ph.D. degree in automatic control from the CICESE Research Center, Ensenada, Mexico, in 2002.

He was a Postdoctoral Fellow with the Université de Liège, Liège Sart Tilman, Belgium, from 2004 to 2005 under the supervision of Prof. R. Sepulchre. He is currently with the Centro de Investigacin y Desarrollo de Tecnología Digital del Instituto Politécnico Nacional (CITEDI-IPN), Tijuana, Mexico. His main research interests include control of electromechanical systems.

Rodolphe Sepulchre received the Engineering and Ph.D. degrees in applied mathematics from the University of Louvain, Louvain-la-Neuve, Belgium, in 1990 and 1994, respectively.

From 1994 to 1996, he held a postdoctoral position at the University of California, Santa Barbara. In 2002–2003, he held a visiting position at Princeton University, Princeton, NJ. He is currently a Professor with the Department of Electrical Engineering and Computer Science, Université de Liège, Liège Sart Tilman, Belgium. He has been a Consultant for Schneider Toshiba since 1999. His research includes theory and control applications of nonlinear dynamical systems.

Authorized licensed use limited to: Rodolphe Sepulchre. Downloaded on May 8, 2009 at 00:30 from IEEE Xplore. Restrictions apply.